Volume 61
Number 35
2 May 2025
Pages 6381–6544

ChemComm

Chemical Communications

rsc.li/chemcomm

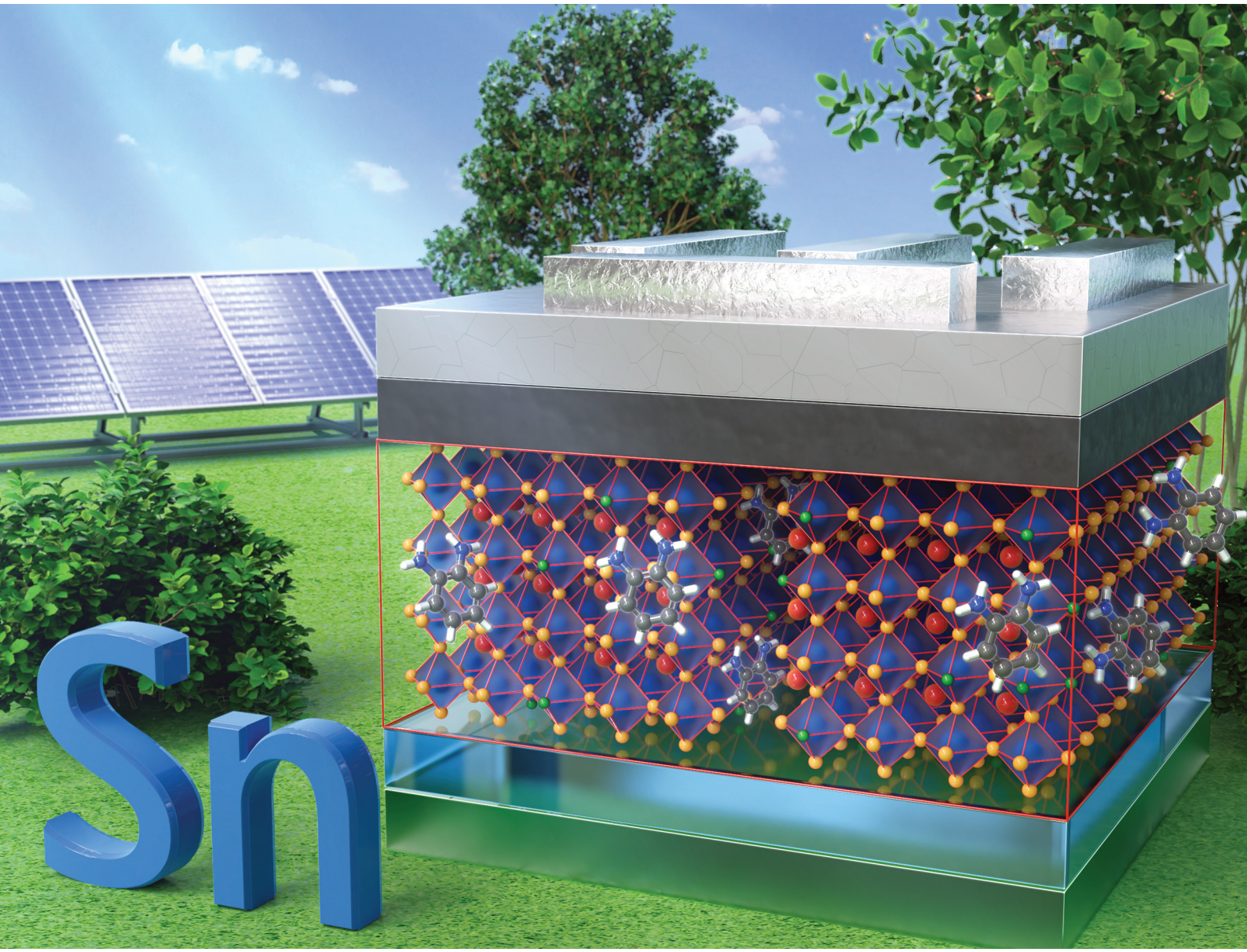

ISSN 1359-7345

ROYAL SOCIETY OF CHEMISTRY

COMMUNICATION

Yuko Takeoka *et al.*

Mitigating low-dimensional phases and defects with methylammonium chloride in high-performance Dion–Jacobson quasi-2D tin perovskite solar cells with power conversion efficiency over 6%

ChemComm

COMMUNICATION

View Article Online
View Journal | View Issue

Cite this: *Chem. Commun.*, 2025, **61**, 6462

Received 3rd March 2025,
Accepted 31st March 2025

DOI: 10.1039/d5cc01145k

rsc.li/chemcomm

Mitigating low-dimensional phases and defects with methylammonium chloride in high-performance Dion–Jacobson quasi-2D tin perovskite solar cells with power conversion efficiency over 6%†

Chunqing Li, [a] Towhid H. Chowdhury, [a] Masahiro Yoshizawa-Fujita, [a] Masahiro Rikukawa, [a] Masatoshi Yanagida, [b] Yasuhiro Shirai [b] and Yuko Takeoka *[a]

Methylammonium chloride (MACl) enhances the performance of Dion–Jacobson quasi-2D tin perovskite solar cells by suppressing low-dimensional phases and defects. The addition of an optimal amount of MACl (20 mol%) improves the crystallinity, film morphology, and charge transport of the quasi-2D tin perovskite layer and enhances the power conversion efficiency (PCE) from 2.9% to 6.2%.

Tin perovskites (TPs) have emerged as a promising alternative to lead perovskites due to their lower toxicity and favorable electronic properties, such as a narrow bandgap and high carrier mobility, which makes them attractive for optoelectronic applications including solar cells, light-emitting diodes, and photodetectors.[1,2] However, the instability of TPs has hindered their widespread commercialization and application.[3–5] A promising strategy to enhance the structural and environmental stability of perovskite materials is the introduction of a two-dimensional (2D) structure.[6–8] Monovalent or divalent organic cations are employed to separate the three-dimensional (3D) perovskite slabs, whereby two general 2D perovskites, Ruddlesden–Popper (RP) and Dion–Jacobson (DJ) types, are formed.[9–11] These types, denoted by the respective formulas of $A_2'A_{n-1}B_nX_{3n+1}$ and $A''A_{n-1}B_nX_{3n+1}$, use organic cations (A′ = monovalent, A″ = divalent) and various combinations of metal (Sn^{2+} or Pb^{2+}) and halide (Cl^-, Br^-, and I^-) components. Here, n represents the number of inorganic layers between two organic spacers ($n = 1$ for pure 2D perovskite, $n > 1$ for quasi-2D perovskite, $n = \infty$ for 3D perovskite).[12,13]

Among these, DJ-type perovskites exhibit enhanced stability compared to RP-type perovskites due to their unique structural characteristics. These include a more uniform and compact inorganic stack with better alignment and less displacement, strong hydrogen bonds within unit cells, intrinsic hydrophobicity of organic spacers, and reduced ion migration rates.[7,14] More importantly, the shortened inter-slab distance between the inorganic plates lowers the charge transfer barrier, which promotes charge transport in these 2D perovskites. Despite these advantages, quasi-2D TPs face significant challenges during formation, such as a non-uniform phase distribution, low-n phases with wide bandgaps and poor charge transport, defects at grain boundaries and tin vacancies.[15] These issues lead to increased defect densities, which affects both the PCE and the stability of the overall tin perovskite solar cell (TPSC).[16–18]

Additive engineering has emerged as an effective solution to control crystallization, enhance film quality, and suppress undesired phases.[19] Sheikh *et al.* showed that chloride played an important role in improving surface coverage of perovskite films with large and uniform grains.[20] Among the various chloride-containing additives, MACl has shown promise for improvement of the crystallization dynamics and structural properties of lead perovskites. Zhao *et al.* reported that MACl may enhance the absorption and coverage of $CH_3NH_3PbI_3$.[21] Mu *et al.* showed that MACl acts as a transitional stabilizer that preserves the crystal structure and facilitates the formation of black-phase formamidinium (FA)-based perovskites.[22] Min *et al.* reported that the MACl additive could stabilize an intermediate phase that led to the formation of pure α-$FAPbI_3$ without annealing through cationic site substitution.[23] However, the effect of MACl on lead-free quasi-2D TPs remains unexplored.

Here, we systematically investigate the role of MACl in DJ-type quasi-2D TPs to address the dual challenges of low-dimensional phase suppression and defect passivation. The quasi-2D perovskites with high n value ($n = 4$ in our case) used in this study were prepared by a spin-coating method with antisolvent treatment. The DJ-type spacer *ortho*-phenylenediamine (*o*-PDA) with a large dipole

[a] *Faculty of Science and Engineering, Sophia University, 7-1 Kioi-cho, Chiyoda-ku, Tokyo, 102-8554, Japan. E-mail: y-tabuch@sophia.ac.jp*
[b] *Photovoltaic Materials Group, Center for GREEN Research on Energy and Environmental Materials, National Institute for Materials Science (NIMS), 1-1 Namiki, Tsukuba, Ibaraki, 305-0044, Japan*

† Electronic supplementary information (ESI) available. See DOI: https://doi.org/10.1039/d5cc01145k

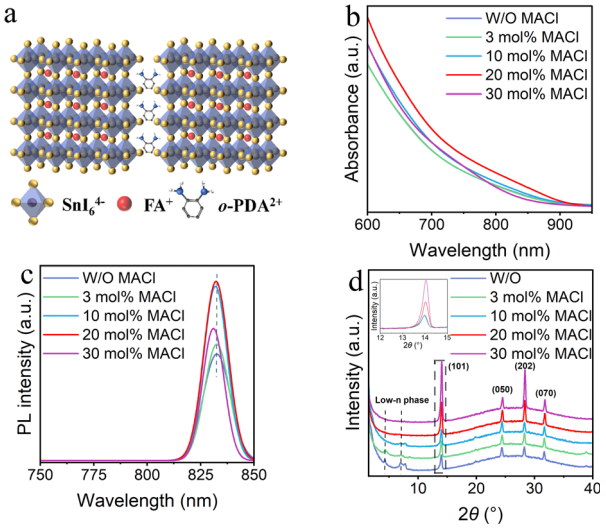

Fig. 1 (a) Schematic representation of estimated DJ structure of quasi-2D perovskites using *o*-PDA. (b) UV-vis absorption spectra, (c) PL spectra, and (d) XRD patterns of the quasi-2D TP with different concentrations of MACl.

moment, which can reduce dielectric mismatch and exciton binding energy, was used as a large organic cation spacer to form *o*-$PDAFA_3Sn_4I_{13}$.[24] The envisaged schematic structure is shown in Fig. 1a. The incorporation of MACl at different molar ratios (3, 10, 20, and 30 mol%) improved both the optical and structural properties of the DJ-type quasi-2D TPs.

Fig. 1b and Fig. S1 (ESI†) presents UV-vis absorption spectra of quasi-2D perovskite films with various MACl concentrations, defined by the molar ratio of MACl to formamidinium iodide (FAI) in the precursor solution. The pristine film without MACl (W/O) exhibits characteristic 3D absorption at approximately 830 nm, with no distinct peaks observed in the low-wavelength region, which is typically associated with low-dimensional phases. This phenomenon is attributed to the high formation energy of the *ortho*-structure of phenylenediamine. Furthermore, the substantial mismatch between the $-CH_2-CH_2-NH_3^+$ group in the *ortho*-structure and adjacent octahedral voids in the perovskite lattice impedes structural compatibility, which suggests that it is difficult for the *ortho*-structure to form a perovskite with an $n = 1$ phase. The geometric incompatibility of the *ortho*-system hinders the formation of low-dimensional phases.[19,25] The UV-vis absorption spectra show a significant enhancement in absorption in the 800–900 nm wavelength range upon the addition of MACl, whereby a maximum is reached at 20 mol% MACl. Fig. 1c presents steady-state photoluminescence (PL) spectra of pristine films and those with MACl. The PL intensity of the emission peak at 830 nm is enhanced in the films that contain the additive, which is likely due to suppressed non-radiative recombination.[26] However, the PL spectra of the quasi-2D TP film with 30 mol% MACl suggested that excessive additive induces non-radiative recombination states within the films; additional defect states or traps promote non-radiative recombination, which leads to energy loss as heat instead of light emission, thereby diminishing the PL intensity.[27,28] To demonstrate the role of MACl in the perovskite precursor solution, the crystallinity of as-spun quasi-2D TP films was examined using X-ray diffraction (XRD), as shown in Fig. 1d. Diffraction peaks were observed at 4.2° and 7.8° for the pure *o*-PDA-based film, which correspond to the $n = 2$ and $n = 1$ phases, respectively. Peaks at 14° and 28° were attributed to the (101) and (202) crystalline planes of high-*n* phases with a structure like 3D $FASnI_3$. The intensity of these low-*n* phases peaks is notably reduced with increasing MACl concentration. Although the intrinsic properties of *o*-PDA limit the formation of low-*n* phases, their occurrence remains inevitable during perovskite film fabrication. However, the introduction of MACl effectively suppresses the formation of these low-*n* phases. Furthermore, the intensity of high-angle peaks increases in MACl-treated films compared to the pristine films. The variations in peak intensity observed in the XRD patterns indicate that crystallization in quasi-2D TP films is enhanced by the presence of MACl during annealing. This modification can most likely be attributed to the influence of MACl in the precursor solution on the crystal growth orientation for the respective perovskite film.

Scanning electron microscopy (SEM) observations were conducted to gain deeper insight into the morphological effects that contribute to enhanced performance with the MACl additive. For simplicity in this analysis, all MACl relevant measurements were performed based on the optimal concentration (20 mol%). The SEM images in Fig. 2a and b compare perovskite films without MACl and those treated with 20 mol% MACl (for other concentrations, see Fig. S2, ESI†). The surface SEM image of the film without MACl reveals pinholes and poor film coverage, which are detrimental to the overall performance of the perovskite layer.[29] In contrast, the SEM image of the film with MACl reveals significant improvements in surface coverage and film uniformity. The enlarged grain size also has the potential to improve the performance of the quasi-2D TP layer. MACl plays a crucial role in improving the perovskite film

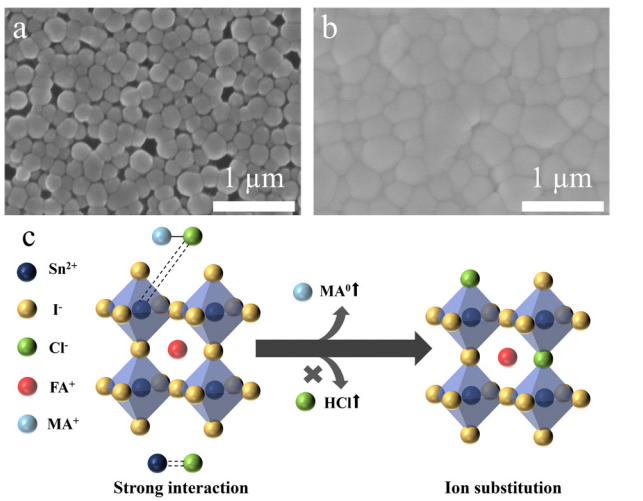

Fig. 2 Top-view SEM images of (a) perovskite film without MACl, and (b) perovskite film treated with 20 mol% MACl. (c) Schematic diagram of effect of MACl.

quality by reducing pinholes and defects. The presence of fewer defects and more complete surface coverage enhances charge transport, which ultimately improves the optoelectronic properties of the film. The observed improvements can be attributed to a dual role of MACl during the fabrication process. First, MACl reduces the crystallization rate during the antisolvent-assisted spin-coating process, which suppresses grain boundary formation and enhances film uniformity.[30] Second, the effect of MACl in TPs differs from that in lead systems due to the unique interaction between Sn^{2+} and Cl^- (Fig. 2c). In TPs, the stronger affinity between Sn^{2+} and Cl^-, as explained by the hard and soft acids and bases (HSAB) theory, allows Cl^- ions to partially remain in the final perovskite structure rather than volatilizing completely during annealing.

These Cl^- ions act as a bridge between Sn^{2+} centres on separate crystallites, which promotes the merging of crystallites and the formation of larger grains. This bridging effect not only enhances the compactness and uniformity of the film but also contributes to the reduction of pinholes and defects, which improves the overall quality and performance of the perovskite layer.

The quasi-2D TP films were investigated using X-ray photoelectron spectroscopy (XPS) to further evaluate the influence of MACl addition on the electronic structure. The XPS spectra (Fig. 3a and b) show characteristic peaks associated with the Sn 3d core at 485.2 and 493.5 eV for Sn^{2+}, and at 486.2 and 494.3 eV for Sn^{4+}.[31,32] Analysis of the deconvoluted peaks reveals that the perovskite film without MACl exhibits a higher ionic percentage (12.31%) of Sn^{4+} compared to the film with 20 mol% MACl (3.90%). This suggests that MACl effectively mitigates the oxidation of Sn^{2+}, thereby enhancing the overall quality of the perovskite film. The I_{3d} binding energy for the perovskite film with 20 mol% MACl was also shifted to higher position compared to the film without MACl, which confirms the passivation of electronic defects (Fig. S3a, ESI†). Moreover, the XPS results, and cross-sectional elemental mapping (EDX) confirm the successful incorporation of chloride ions into the perovskite lattice (as shown in Fig. S3b and S4, ESI†), which provides critical insight into their role in d effect passivation and the suppression of Sn^{2+} oxidation.

To assess the photovoltaic performance of quasi-2D TPSCs, inverted solar cells with an indium tin oxide (ITO)/poly(3,4-ethylene dioxythiophene):poly(styrene sulfonate) (PEDOT:PSS)/quasi-2D TP/[6,6]-phenyl-C_{61}-butyric acid methyl ester (PCBM)/

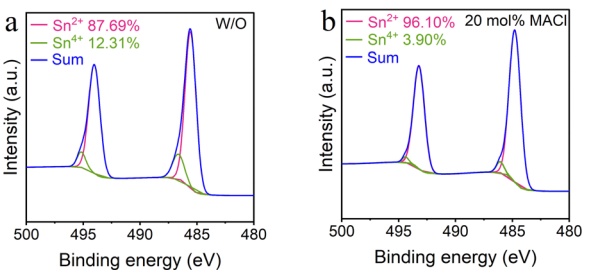

Fig. 3 XPS spectra: (a) and (b) Sn 3d of the perovskite without and with 20 mol% MACl.

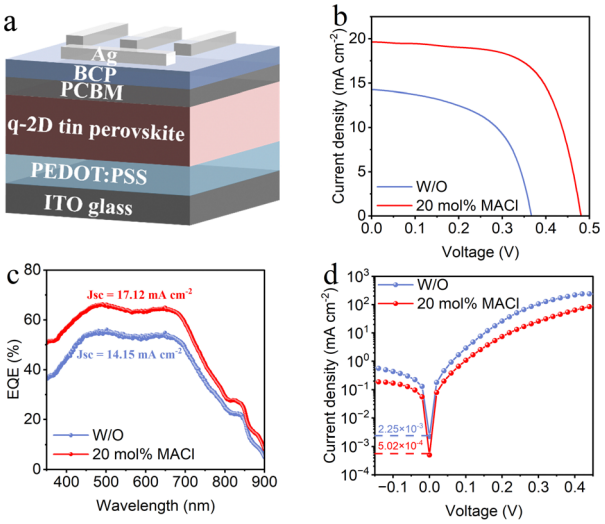

Fig. 4 (a) Device structure for quasi-2D TPSCs. (b) *J*–*V* curves, (c) EQE, and (d) dark *J*–*V* curves for champion devices for quasi-2D TPSCs treated with and without 20 mol% MACl.

bathocuproine (BCP)/Ag structure (Fig. 4a) were fabricated. The corresponding *J*–*V* curves and photovoltaic parameters are presented in Fig. 4b, Fig. S5 and Table S1 (ESI†). The device based on the perovskite layer without MACl exhibited a PCE of 2.90% with an open-circuit voltage (V_{OC}) of 0.36 V, a short-circuit current density (J_{SC}) of 14.29 mA cm^{-2}, and a fill factor (FF) of 0.55. The incorporation of 20 mol% MACl significantly increased the PCE to 6.20%, with enhanced parameters (V_{OC} to 0.48 V, J_{SC} to 19.62 mA cm^{-2}, and FF to 0.66). 20 mol% of MACl induces preferential orientation during perovskite crystallization and suppresses defect formation, improving film morphology and crystallinity, resulting in higher V_{OC} in the respective PSCs. MACl also suppresses low-dimensional phases, leading to more efficient charge transport and facilitates improved J_{SC} and FF. These combined effects contribute to the significant enhancement of photovoltaic performance in the 20 mol% MACl-based devices. However, excessive MACl can disrupt the film uniformity, as illustrated in Fig. S2 (ESI†), by the formation of more defects or uneven crystallization that negatively impact device performance. Although MACl improves performance by passivating defects, hysteresis persists due to ion migration, charge accumulation at interfaces, and perovskite film properties. Chloride ion migration may affect charge distribution, while interfacial charge accumulation and recombination contribute to hysteresis, especially under reverse bias. The statistical data in Fig. S6 (ESI†) demonstrates that devices with incorporated MACl exhibit narrower parameter distributions across batches compared to the control device, which suggests enhanced reproducibility and improved overall performance. Fig. 4c shows the external quantum efficiency (EQE) of the device without MACl and the best quasi-2D TPSCs with 20 mol% MACl. The EQE spectrum for the device with 20 mol% MACl reveals a noticeable enhancement across the entire spectral range, which indicates the suppression of recombination activity in the bulk and at the

interfaces in the device.[33] The J_{SC} values (14.15 mA cm^{-2} for W/O and 17.12 mA cm^{-2} for the device with 20 mol% MACl) obtained by integration of the EQE spectrum are close to those obtained from the *J–V* curves. The lower dark current for the device treated with MACl further supports effective defect passivation (Fig. 4d) because a high dark current is typically associated with an increased defect density. Light intensity-dependent V_{OC} measurements (Fig. S7, ESI†) yielded slopes of $1.79kT/q$ and $3.35kT/q$ for the devices with and without MACl, respectively. Deviation from kT/q suggests trap-assisted Shockley–Read–Hall (SRH) recombination, where a smaller slope indicates reduced trap-assisted recombination. These results confirm that 20 mol% of MACl suppresses non-radiative recombination, which explains the high V_{OC} of the respective PSC. A long-term stability was investigated on unencapsulated devices in an ambient environment and the results are shown in Fig. S8 (ESI†). The PCE for the quasi-2D TPSC with 20 mol% MACl retained over 85% of its initial value after storage for 600 h, whereas that for the untreated device decreased to 70% under the same conditions. This enhanced stability is attributed to the incorporation of MACl, which effectively passivates defects and charge traps within the perovskite film, thereby reducing non-radiative recombination and improving film durability.

In conclusion, this study demonstrates that MACl plays a critical role in enhancement of the performance of DJ-type quasi-2D TPSCs by suppressing low-dimensional phases and passivating defects. The optimized incorporation of MACl (20 mol%) improves film crystallinity, reduces non-radiative recombination, and enhances charge transport, which leads to a significant increase in power conversion efficiency from 2.90% to 6.20%. Structural and optical analyses confirm that MACl modifies the crystallization process, suppresses the formation of low-*n* phases, and enhances film morphology. These results offer a viable strategy for improving the performance of DJ-type quasi-2D TPSCs.

This work was supported in part by the Japan Science and Technology Agency (JST)-ALCA-Next Program (Grant No. JPMJAN23B2).

Data availability

Data supporting this article have been included in the ESI.†

Conflicts of interest

There are no conflicts to declare.

Notes and references

1 F. Hao, C. C. Stoumpos, D. H. Cao, R. P. H. Chang and M. G. Kanatzidis, *Nat. Photonics*, 2014, **8**, 489–494.
2 N. K. Noel, S. D. Stranks, A. Abate, C. Wehrenfennig, S. Guarnera, A. A. Haghighirad, A. Sadhanala, G. E. Eperon, S. K. Pathak, M. B. Johnston, A. Petrozza, L. M. Herz and H. J. Snaith, *Energy Environ. Sci.*, 2014, **7**, 3061–3068.
3 M. I. Saidaminov, I. Spanopoulos, J. Abed, W. J. Ke, J. Wicks, M. G. Kanatzidis and E. H. Sargent, *ACS Energy Lett.*, 2020, **5**, 1153–1155.
4 J. K. Liu, H. H. Yao, S. R. Wang, C. Wu, L. M. Ding and F. Hao, *Adv. Energy Mater.*, 2023, **13**, 2300696.
5 X. Zhang, S. R. Wang, W. K. Zhu, Z. Y. Cao, A. L. Wang and F. Hao, *Adv. Funct. Mater.*, 2022, **32**, 2108832.
6 Y. Q. Liao, H. F. Liu, W. J. Zhou, D. W. Yang, Y. Q. Shang, Z. F. Shi, B. H. Li, X. Y. Jiang, L. J. Zhang, L. N. Quan, R. Quintero-Bermudez, B. R. Sutherland, Q. X. Mi, E. H. Sargent and Z. L. Ning, *JACS*, 2017, **139**, 6693–6699.
7 S. Y. Shao, J. J. Dong, H. Duim, G. H. ten Brink, G. R. Blake, G. Portale and M. A. Loi, *Nano Energy*, 2019, **60**, 810–816.
8 F. Wang, X. Y. Jiang, H. Chen, Y. Q. Shang, H. F. Liu, J. L. Wei, W. J. Zhou, H. L. He, W. M. Liu and Z. J. Ning, *Joule*, 2018, **2**, 2732–2743.
9 L. L. Mao, W. J. Ke, L. Pedesseau, Y. L. Wu, C. Katan, J. Even, M. R. Wasielewski, C. C. Stoumpos and M. G. Kanatzidis, *JACS*, 2018, **140**, 3775–3783.
10 D. Lu, G. W. Lv, Z. Y. Xu, Y. X. Dong, X. F. Ji and Y. S. Liu, *JACS*, 2020, **142**, 11114–11122.
11 M. Rahil, R. M. Ansari, C. Prakash, S. S. Islam, A. Dixit and S. Ahmad, *Sci. Reports*, 2022, **12**, 2176.
12 M. Akiyoshi, M. Yoshizawa-Fujita, Y. Takeoka and M. Rikukawa, *Chem. Commun.*, 2021, **57**, 3395–3398.
13 R. Hamaguchi, M. Yoshizawa-Fujita, T. Miyasaka, H. Kunugita, K. Ema, Y. Takeoka and M. Rikukawa, *Chem. Commun.*, 2017, **53**, 4366–4369.
14 F. Z. Li, J. Zhang, S. Jo, M. C. Qin, Z. Li, T. T. Liu, X. H. Lu, Z. L. Zhu and A. K. Y. Jen, *Small Methods*, 2020, **44**, 23188–23196.
15 Y. T. Zheng, T. T. Niu, J. Qiu, L. F. Chao, B. X. Li, Y. G. Yang, Q. Li, C. Q. Lin, X. Y. Gao, C. F. Zhang, Y. D. Xia, Y. H. Chen and W. Huang, *Solar RRL*, 2019, **3**, 1900090.
16 Y. Lin, Y. J. Fang, J. J. Zhao, Y. C. Shao, S. J. Stuard, M. M. Nahid, H. Ade, Q. Wang, J. E. Shield, N. H. Zhou, A. M. Moran and J. S. Huang, *Nat. Commun.*, 2019, **10**, 1008.
17 N. Zhou, Y. H. Shen, L. Li, S. Q. Tan, N. Liu, G. H. J. Zheng, Q. Chen and H. P. Zhou, *JACS*, 2018, **140**, 459–465.
18 X. Zhang, R. Munir, Z. Xu, Y. C. Liu, H. Tsai, W. Y. Nie, J. B. Li, T. Q. Niu, D. M. Smilgies, M. G. Kanatzidis, A. D. Mohite, K. Zhao, A. Amassian and S. Z. Liu, *Adv. Mater.*, 2018, **30**, 1707166.
19 B. B. Yu, L. M. Xu, M. Liao, Y. H. Wu, F. Z. Liu, Z. F. He, J. Ding, W. Chen, B. Tu, Y. Lin, Y. D. Zhu, X. S. Zhang, W. T. Yao, A. B. Djurisic, J. S. Hu and Z. B. He, *Solar RRL*, 2019, **3**, 1800290.
20 M. A. K. Sheikh, R. Abdur, S. Singh, J. H. Kim, K. S. Min, J. Kim and J. Lee, *Electron. Mater. Lett.*, 2018, **14**, 700–711.
21 Y. X. Zhao and K. Zhu, *J. Phys. Chem. C*, 2014, **118**, 9412–9418.
22 C. Mu, J. L. Pan, S. Q. Feng, Q. Li and D. S. Xu, *Adv. Energy Mater.*, 2017, **7**, 1601297.
23 H. Min, M. Kim, S. U. Lee, H. Kim, G. Kim, K. Choi, J. H. Lee and S. I. Seok, *Science*, 2019, **366**, 749–753.
24 H. H. Yao, T. Wu, C. Wu, L. M. Ding, Y. Hua and F. Hao, *Adv. Energy Mater.*, 2024, **34**, 2312287.
25 C. Liu, Y. Yang, K. Rakstys, A. Mahata, M. Franckevicius, E. Mosconi, R. Skackauskaite, B. Ding, K. G. Brooks, O. J. Usiobo, J. N. Audinot, H. Kanda, S. Driukas, G. Kavaliauskaite, V. Gulbinas, M. Dessimoz, V. Getautis, F. De Angelis, Y. Ding, S. Y. Dai, P. J. Dyson and M. K. Nazeeruddin, *Nat. Commun.*, 2021, **12**, 6394.
26 X. Li, D. Q. Bi, C. Y. Yi, J. D. Decoppet, J. S. Luo, S. M. Zakeeruddin, A. Hagfeldt and M. Grätzel, *Science*, 2016, **353**, 58–62.
27 D. B. Khadka, Y. Shirai, M. Yanagida, T. Tadano and K. Miyano, *Chem. Mater.*, 2023, **35**, 4250–4258.
28 Y. Su, J. Yang, G. L. Liu, W. P. Sheng, J. Q. Zhang, Y. Zhong, L. C. Tan and Y. W. Chen, *Adv. Funct. Mater.*, 2022, **32**, 2109631.
29 W. Q. Liao, D. W. Zhao, Y. Yu, C. R. Grice, C. L. Wang, A. J. Cimaroli, P. Schulz, W. W. Meng, K. Zhu, R. G. Xiong and Y. F. Yan, *Adv. Mater.*, 2016, **28**, 9333–9340.
30 J. Park, J. Kim, H. S. Yun, M. J. Paik, E. Noh, H. J. Mun, M. G. Kim, T. J. Shin and S. I. Seok, *Nature*, 2023, **616**, 724–730.
31 J. F. Chen, J. F. Luo, E. L. Hou, P. Q. Song, Y. Q. Li, C. Sun, W. J. Feng, S. Cheng, H. Zhang, L. Q. Xie, C. B. Tian and Z. H. Wei, *Nat. Photonics*, 2024, **18**, 464–470.
32 D. B. Khadka, Y. Shirai, M. Yanagida and K. Miyano, *J. Mater. Chem. C*, 2020, **8**, 2307–2313.
33 A. Nakane, H. Tampo, M. Tamakoshi, S. Fujimoto, K. M. Kim, S. Kim, H. Shibata, S. Niki and H. Fujiwara, *J. Appl. Phys.*, 2016, **120**, 064505.